NUCLEAR INSTRUMENTS AND METHODS 147 (1977) 487-499 ; © NORTH-HOLLAND PUBLISHING CO.

HIAWATHA, A FISSION-FRAGMENT RECOIL MASS SPECTROMETER† *

GINO DIIORIO+ and B. W. WEHRING

Nuclear Engineering Program, University of Illinois at Urbana-Champaign, Urbana, Illinois 61801, U.S.A.

Received 20 May 1977 and in revised form 28 June 1977

A new fission-fragment recoil mass spectrometer, called HIAWATHA, has been designed, constructed, and tested. Working on a unique principle, HIAWATHA has achieved better than 0.5 amu mass resolution measuring fragments directly from fission. The good mass resolution obtained by HIAWATHA permitted us to make a direct physical measurement of the mass yields in thermal-neutron fission of ^{235}U. The results of this measurement are in good agreement in general with evaluated mass yields. Future experiments planned for HIAWATHA include measurements of the *mass* yields for thermal-neutron fission of ^{233}U and ^{239}Pu, measurements of the *nuclide* yields for all three of the fissile isotopes by incorporating a fragment energy-loss detector for atomic-number identification, and various studies of heavy-ion transport in matter.

1. Introduction

Most fission product yield data is based on the techniques of radiochemistry and indirect mass spectrometry. These techniques have enabled the determination of mass chain yields but have been incapable of obtaining a complete set of fission nuclide yield data. Measurements for thermal fission of ^{235}U, the most abundant and precise, for all the fissioning processes, have been performed on less than half of the significant nuclide yields with experimental uncertainties of less than 50%. For other fissile isotopes, yields are known less accurately[1,2]).

In order to check for systematic errors in present evaluated yields and to obtain a complete set of fission yields for all thermal-neutron fission, an alternate method has been developed. The method is a direct physical measurement employing a new fission-fragment recoil mass spectrometer. This unique spectrometer, which we call HIAWATHA, has achieved 0.5 amu mass resolution for both light and heavy fission fragments[3]). The best mass resolution previously obtained by others in similar experiments is 2–3 amu[4-6]). The mass resolution obtained by HIAWATHA allows exact mass identification and, therefore, accurate mass-yield measurements[7]). It also permits fragment atomic number identification by fragment energy loss and, therefore, accurate nuclide-yield measurements. Both exact mass identification and atomic-number identification by energy loss requires a mass resolution significantly better than 1 amu.

Some other types of spectrometer systems, whose construction was spurred by the interest in fission product study, are of a more conventional nature. Fission fragment on-line separators such as Tristan and Osiris employ magnetic mass spectrometers whose ion source emits fission fragments that have been stopped by an absorber and transported to the source filament[8]). Although times from fission to detection of less than a second are possible, on-line separators are not used for fission-yield measurements because of large differences in efficiencies for different elements.

Fission-fragment recoil mass spectrometers measure fragments recoiling directly from fission eliminating elemental selectivity associated with ion sources. Unlike the ion source of a conventional mass spectrometer, however, the fission source of a recoil mass spectrometer emits ions possessing a wide range of ionic charge states and kinetic energies as well as a range of atomic masses. Recoil spectrometers of the parabolic type[9,10]) using magnetic and electrostatic analyzers have been constructed for fission product study. The parabolic type spectrometer separates fragments on the basis of mass-to-ionic charge ratio. Exact mass identification can be made only where the ratios can be resolved. Because of the large fields necessary for analyzing the fragments, the spectrometer is a costly system to build and consequently only several in the world have been built, the Lohen-

* Research supported by a grant from the U.S. National Science Foundation.

† This article is based on a portion of a dissertation by one of the authors (GD) submitted in partial fulfillment of the requirements for the doctoral degree at the University of Illinois.

+ Present address: Applied Physics Division, Argonne National Laboratory, Argonne, Illinois 60439, U.S.A.

grin facility at Grenoble being the most productive[10,11]).

The design criterion for HIAWATHA was that the spectrometer should be able to resolve fission-fragment masses to less than 1 amu. This resolution is essential for obtaining accurate yields from fission. The concept of our method is an extension of the single time-of-flight experiment, where the time-of-flight t fragments take to traverse a distance d and the kinetic energy E of the fragment are measured. The mass m of the fragment is determined through the kinetic energy relationship: $E = \frac{1}{2}m\,(d/t)^2$.

For time-of-flight experiments a variety of "zero-time" detectors have been used with surface-barrier detectors, with the best time resolutions reported being about 200 ps [12–14]). Therefore, for fission-fragment velocities, flight paths of several meters result in timing uncertainties smaller than 1%. However, energy resolution of surface-barrier detectors is only 2–4% for fission fragments and is the limiting factor for achieving less than one-amu mass resolution for fission products.

The problem of energy resolution was solved by the use of an electrostatic analyzer in the flight path. The analyzer deflects particles on the basis of kinetic-energy-to-ionic-charge ratio and, in principle, can have as fine a resolution as desired. The energy resolution chosen was 0.3%. The analyzer alone, however, was not enough to identify the fragment energy. Fission fragments are born with a spectrum of charge states and the analyzer transmits a different energy for each of these charge states for any given high voltage setting. A surface-barrier detector was needed to identify the approximate kinetic energy of the fragment. Because charge states are exactly integers, the fragment energy was determined precisely from the approximate kinetic energy as measured by the surface-barrier detector and a knowledge of the analyzer high voltage. Surface-barrier detector energy resolutions are sufficient for the most part to resolve adjacent charge states. Typical charge state separations for fragments range from about 3 to 6%[15]).

The introduction of the electrostatic analyzer in the flight path added a problem to velocity determination. Variations in flight length and electric field potentials due to different trajectories in the analyzer limited the velocity resolution of the experiment. To maintain a satisfactory velocity resolution, the acceptance angle of the analyzer was limited. Trajectories were constructed such that a maximum uncertainty of 0.2% in velocity was expected. Narrow acceptance angles were detrimental to count rates but aided in analyzer construction. Narrow plate separation allowed the maximum field strength required to be obtained with a potential of 110 kV.

In order to test HIAWATHA, mass yields were measured for the thermal-neutron fission of ^{235}U [7]). This measurement also served to reduce the uncertainties in the present mass-yield data and to check against systematic errors associated with the methods used to arrive at fission-fragment yields, radiochemistry and indirect mass spectrometry. Since a direct physical measurement is not subject to the same types of errors as indirect chemical measurements, the results of the HIAWATHA measurement when compared with previous results give the most accurate mass-yield data for thermal-neutron fission of ^{235}U.

In addition to increasing the accuracy of present mass-yield data for thermal-neutron fission of ^{235}U, the HIAWATHA results showed that such measurements for thermal-neutron fission of ^{239}Pu and ^{233}U will be important since these mass yields are not as well known as those for ^{235}U. Also, the HIAWATHA results demonstrated the feasibility of using HIAWATHA in direct physical measurements of nuclide yields in thermal-neutron fission for all three isotopes.

2. Experimental apparatus

2.1. Physical arrangement

The layout of the fission-fragment recoil mass spectrometer HIAWATHA is shown in fig. 1. The Illinois Advanced TRIGA Reactor thru neutron beamport is used for HIAWATHA because the location offered the longest floor area for the spectrometer and because the thru beamport is a tangential beamport giving a good ratio of thermal-neutron flux to gamma-and-fast-neutron radiation streaming.

A thin (<1 mg/cm^2) fission foil is located in the center of the thru beamport inside an evacuated 11′2″ i.d. aluminium flight tube which transports the fragments to a "zero-time" chamber. A "zero-time" detector in this chamber detects the passage of fragments giving a signal marking the beginning of the time of flight, while allowing the fragment to proceed with minimal perturbations. The fragments then pass through a flight tube of

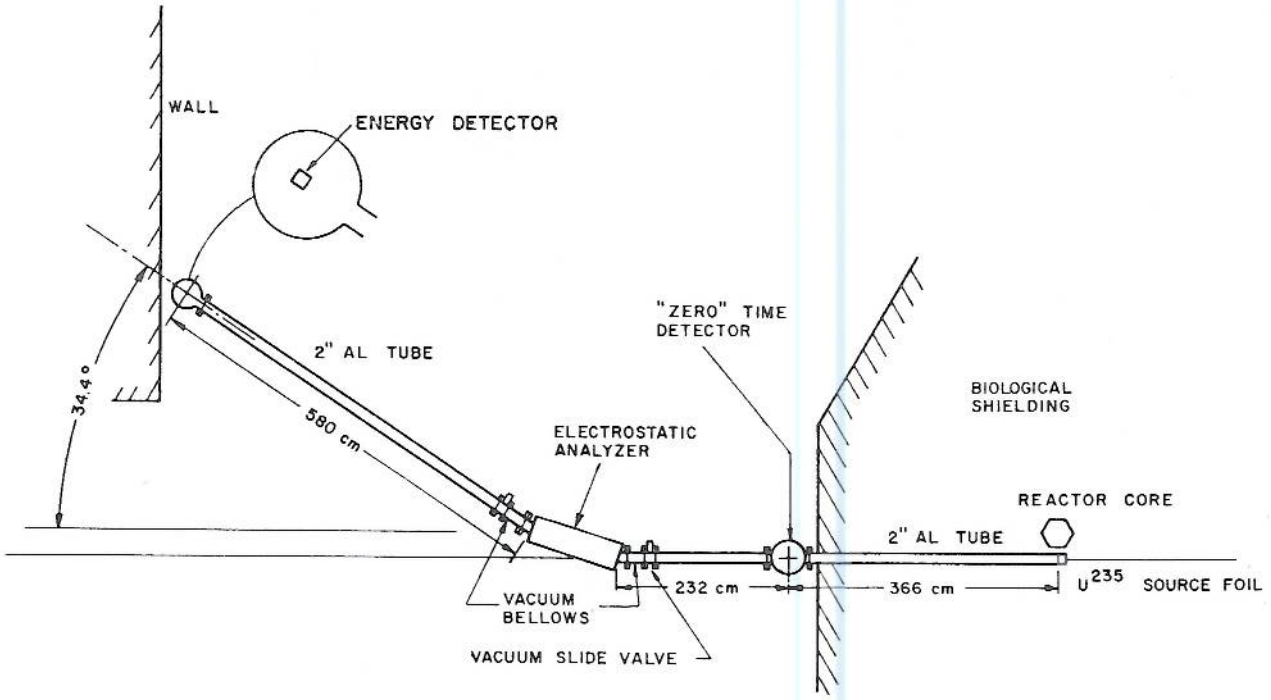

Fig. 1. Arrangement for experiments using the fission-fragment recoil mass spectrometer HIAWATHA and the Illinois Advanced TRIGA nuclear reactor.

232 cm length where they enter the electrostatic analyzer. Those fragments selected by the analyzer are deflected 34.4° in a horizontal plane, and exit into a 580 cm long flight tube. Fragments are stopped at the end of the path by a surface-barrier detector.

The system was designed so that the source could be removed to allow other researchers the use of the beamport facility. The removal of the source from the west side of the thru beamport necessitates the dismantling of the "zero-time" chamber and the tube connecting the time chamber to the analyzer. A vacuum slide valve at the entrance of the analyzer marks the beginning of the permanent section of the spectrometer and allows continual pumping of the analyzer while the source is being loaded or unloaded. A concrete block shielding wall encloses the permanent section of the spectrometer. A hole in the forward wall allows passage of the beam tube and a hole in the back wall allows the passage of the radiation into a beam catcher placed behind the wall.

Three annular shielding plugs made of steel, plexiglass, and lead approximately 4″ in length are placed inside the transport tube to reduce the beam from 2″ to approximately 1″ in diameter. Aluminum baffles are placed close to the source foil holder. These baffles, combined with the shielding plugs, reduce the amount of fission-fragment scattering from the inside of the tube. The placement of the source foil is near the core-graphite reflector boundary of the reactor. The ratio of thermal to fast neutron flux at this location is about unity. At full power operation of 1.5 MW, the thermal neutron flux at the foil is approximately 4×10^{12} neutrons/cm$^2\cdot$s.

2.2. Zero-time detector

There were four major requirements the zero-time detector had to fulfill. Its design and construction were made with these requirements in mind:

1) subnanosecond time resolution,
2) discrimination between fission fragments and background events,
3) high detection efficiency, and
4) minimal scattering of the fragment beam.

A design that fulfilled these requirements was one that was based on the work of Dietz[14]). Fragments pass through a thin (400 Å) carbon foil, which is normal to the beam, and cause ionization in this foil resulting in the liberation of secondary elec-

trons. These electrons are accelerated by an electric field parallel to the beam into a magnetic field. The magnetic field deflects the electrons into a scintillator phototube combination.

The carbon foil was mounted on a foil holder which also served as a fragment beam collimator with a rectangular aperture of 20 mm length by 4.7 mm width. The foil holder was mounted in the center of a rectangular cathode plate and the unit is supported from ground by ceramic insulators. The cathode is charged to a negative 19 kV creating a homogeneous accelerating field. The magnet is a permanent magnet measured to have a magnetic field of 80 G. The electrons are deflected 45° and radially focused to a point on the scintillator surface. By having the photomultiplier tube removed from the radiation beam, the interaction between gammas and neutrons with the scintillator and phototube is greatly reduced. Furthermore, only those electrons born with thermal energies are allowed to reach the scintillator, reducing accidental background from Compton scattered electrons originating at the timing foil and also, variations in electron transit times.

The scintillator was fastened with epoxy on a $\frac{1}{8}''$ thick polished plexiglass disk which serves both to optically couple the scintillator to the photomultiplier tube and to form a vacuum seal against a rubber "O-ring" surface. The photomultiplier tube (56 AVP) was connected to the light pipe with optical grease. The scintillator is 0.010" NE 102 which is thick enough to stop the 19 kV electrons and shift the wavelength of the emission to the region of photomultiplier tube response.

A holder containing a ^{252}Cf source and a surface-barrier detector was mounted on a push–pull vacuum feedthru. In the down position the californium source is situated about 1 cm from the timing foil, blocking the ^{235}U fission-fragment beam. This position is used for testing and calibrating the timing system. The spontaneous fission of californium resulted in one fission fragment passing through the timing foil and its complement being stopped by the energy detector. Time-of-flight differences are on the order of 1–2 ns.

2.3. Electrostatic analyzer

The electrostatic analyzer of HIAWATHA has two cylindrically curved electrodes one at a positive potential and the other at an equal but negative potential. The cylindrical geometry of the electrodes exhibits the property of radial focusing. This means that fragments emerging from a point on the timing foil will be deflected to a point on the surface-barrier detector for any small radial angle with which they emerge. This property was employed to enhance the counting rate for the experiment. The equations governing the behavior of electrostatic analyzers are described by Wollnick[16]).

The electrodes of the electrostatic analyzer were fabricated from two aluminum plates, electropolished, and precision mounted to a common base plate by ceramic insulators (see fig. 2). The plates were rolled from $\frac{3}{16}''$ thick sheets to approximately the radius of curvature and then aligned to the exact radius of curvature by shimming and grinding of the supporting insulators. The insulators

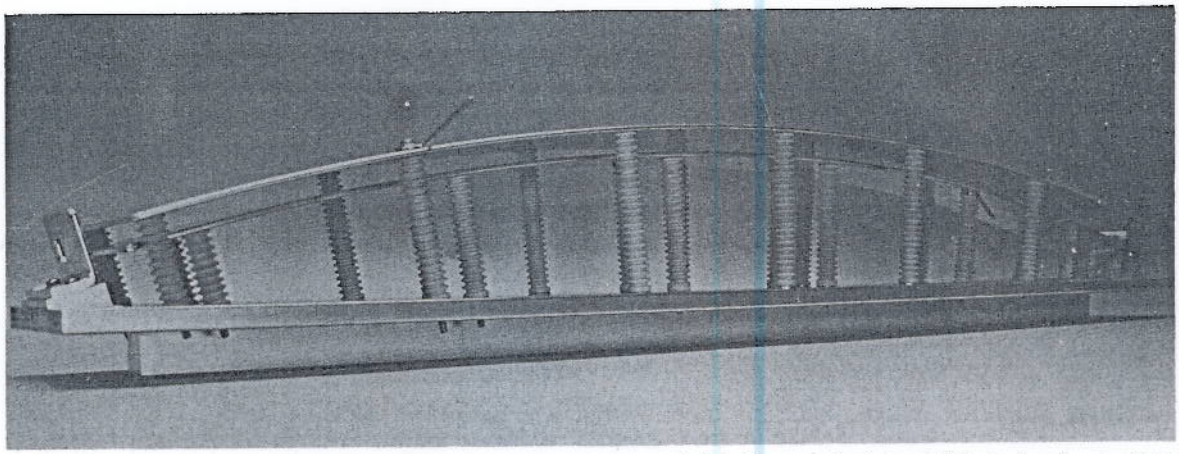

Fig. 2. Electrodes of the electrostatic analyzer composed of two cylindrically curved electropolished aluminum plates supported and insulated from a common baseplate by lavite insulators. Shielding diaphragms at both ends define the beam entrance and exit.

were machined from lavite and then fired to their approximate length. A jig mill was used for the purpose of mounting the electrodes and allowed 0.001″ precision. A dial indicator was used to map the plate spacing to check for gap uniformity. The electrode edges were rounded and the fastenings to the supports were such that there were no sharp edges.

Shielding diaphragms were placed at the entrance and exit of the analyzer to define the field boundary. The effective angle of curvature and radius of curvature are 34.4° and 216 cm, respectively. The gap was 17 mm and the maximum designed potential difference across the gap was 120 kV.

The electrode assembly was mounted inside a chamber such that the axis of curvature was vertical. The vacuum chamber was constructed from a 12″ i.d. aluminum tube with a $\frac{3}{8}$″ wall thickness. All the metallic components of the vacuum vessel and electrode assembly were electropolished to reduce arcing and to reduce the vacuum outgassing load.

Incorporated in the analyzer chamber is a set of carefully positioned apertures through which a laser beam was used to align the system. There are four of these alignment holes: one at each shielding diaphragm and two on an alignment box on the chamber. The hole on the diaphragm and its corresponding hole on the chamber box form a line of sight that is parallel to the fragment beam and displaced 0.750″ from it. A laser cradle on the vacuum chamber held a laser which when properly adjusted allowed the laser beam to pass through the hole pair for alignment purposes. The alignment holes were drilled using a jig mill to establish a position tolerance to 0.010″.

Two Ceramaseal 60 kV high voltage vacuum connectors feed the high voltage into the vacuum chamber. Voltage connection to the electrodes is made by copper tubing. Attachment of the beam tubes to the chamber is made through stainless steel vacuum bellows at the entrance and exit. A 2″ vacuum slide valve was provided at the entrance to allow continual pumping at the analyzer. Also at the forward beam entrance is a 4″ long 4″ i.d. stainless steel nipple housing a surface-barrier detector on a push–pull feedthru. In the down position, the detector was used to monitor the energy spectrum of fragments entering the analyzer.

In selecting the various design parameters many things were considered. The radius of curvature was bounded by space and construction limitations at the large extreme and by excessively high field strengths at the low extreme. Angle of curvature strongly influenced the focal lengths of the system. Aperture widths were based on the criterion that energy resolution should equal 0.3% fwhm. Aperture width ratio and focal length ratios were optimized for high counting rate.

Maximum electrode spacing was limited by field strength requirements and also by time-of-flight considerations. Differences in fragment trajectories in the analyzer gap were the limiting factor in achieving good time resolution for the experiment. Fragments entering the gap close to the anode had a longer flight path than those entering close to the cathode and also experienced a slowing down due to the field. By choosing the beam collimator at the analyzer entrance to be 9.7 mm, the error introduced to time-of-flight resolution was less than 0.2%. Plate spacing was selected such that fragments being analyzed and having diverging paths passed through the analyzer without suffering a collision with the electrodes.

2.4. Energy detector

The energy detector at the end of the fragment flight path is an ORTEC 400 mm² surface-barrier heavy-ion detector. The detector is mounted normal to the beam inside a stainless steel cross. One

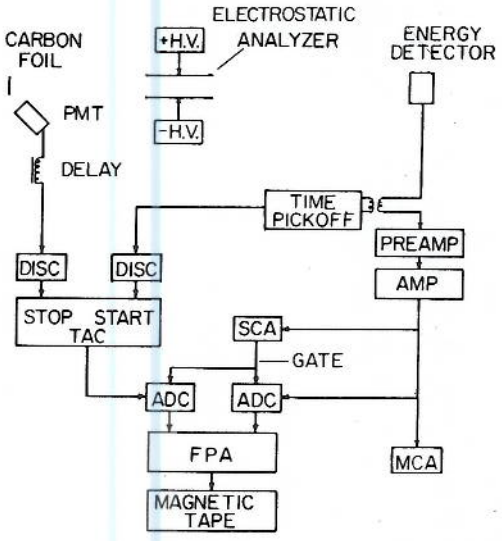

Fig. 3. Schematic diagram of the data collection system. The following abbreviations are used: AMP–amplifier, SCA–single channel analyzer, MCA–multichannel analyzer, ADC–analog-to-digital convertor, DISC–discriminator, TAC–time-to-amplitude convertor, FPA–four-parameter buffer memory/analyzer, and PMT–photomultiplier tube.

leg of the cross is connected to the fragment beam tube through a 2" vacuum slide valve. The oppo- leg of the cross is blanked off with a disk ding the detector, detector mask, and detector crodot electrical feedthrough. The detector ask aperture is rectangular being 20 mm in ngth and 10.3 mm in width.

A push–pull feedthrough mounted on a leg normal to the beam contains a ^{252}Cf fission source. In the down position the source is used to calibrate the detector. In the withdrawn position the californium is enclosed so that contamination of the energy detector by californium self-transfer is minimized.

2.5. Electronic equipment

A block diagram of the electronics used for gathering mass-yield data is shown in fig. 3. Two parameters are required to determine fragment mass: energy and time-of-flight. The energy signal generated by the surface-barrier detector is amplified and shaped by a Tennelec TC 164 preamplifier and a Tennelec TC 214 amplifier. The pulse is then digitized by a Northern Scientific 627 Analog-to-Digital Converter (ADC) and stored in a four-parameter buffer memory/analyzer (FPA)*.

An ORTEC model 467 time-to-amplitude converter (TAC) determines the fragment time-of-flight between the timing foil and the energy detector. The time signal generated at the "zero-time" chamber is delayed by a delay cable with a delay greater than the largest flight time of a fragment so that the time signal derived at the energy detector could be used as the TAC START input. This is done because of the high accidental background rate at the "zero-time" chamber.

The signal at the zero-time detector is derived from the anode of the 56 AVP photomultiplier tube base. The timing signal at the energy detector is obtained by a time pickoff unit[17]) placed between the energy detector and preamplifier. The cable between the energy detector and time pickoff was kept as short as possible to reduce capacitance.

Both timing signals are fed into Chronetics 101 discriminators. The outputs of the discriminators are fed to the TAC, the "zero-time" detector signal to the STOP input and the energy detector time signal to the START input. The TAC output is digitized by an ADC and stored by the FPA. After accumulating 128 events, the data are transferred to 7-track magnetic tape and a new cycle of data acquisition begins. The data are later analyzed off line using the IBM 360 computer facility at the University.

The high voltage of the electrostatic analyzer is supplied by two Spellman 60 kV 0.5 mA power supplies having line, load, and ripple specifications of 0.01%, 0.01% and 0.02%, respectively. A voltage divider reduces the output voltage on the order of 1000:1 for metering purposes. A null voltmeter/standard is used to monitor the analyzer voltage.

3. Testing of HIAWATHA

3.1. Experimental procedure

In order to test the capabilities of HIAWATHA, mass yields were measured for the thermal-neutron fission of ^{235}U and the results compared to the evaluated yield data of Meek and Rider[2]). The experiment was performed by irradiating a 1 mg/cm^2 93%-enriched ^{235}U foil at a steady-state thermal-neutron flux of 4×10^{12} n/cm^2·s in the center of the thru neutron beamport of the Illinois Advanced TRIGA nuclear reactor.

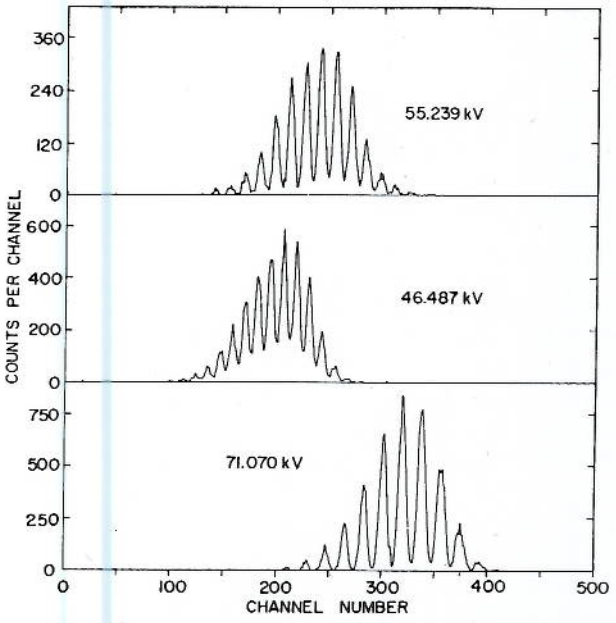

Fig. 4. Pulse-height spectra measured by the surface-barrier detector in HIAWATHA. The electrostatic analyzer voltage setting for each run is given on the graphs. The structure in these spectra is due to the integer charge states of the fragments.

* The FPA was designed and constructed by R. Bucher and one of the authors (GD), to be used in their thesis research.

The source, transport tube, and timing chamber were assembled several days before the start of the experiment and allowed to pump down, after which time, operating pressures at each of three diffusion-pump stations were found to be about 3×10^{-6} torr. An analyzer voltage was selected and measured. A delay cable was selected and a time spectrum gated with the energy signal was obtained from the TAC module and displayed on a multichannel analyzer. This was to insure that the delay was such that all events were within the time range of the TAC.

Once the correct delay cable was selected, the data acquisition began. Events were gated with the energy signal. The four-parameter analyzer (FPA) was switched to a mode where it required only an energy event to process the data. In this way "zero-time" detector inefficiencies were determined. A data collection time of about one hour was sufficient to obtain a good mass distribution for one voltage setting of the electrostatic analyzer. The measurement was repeated for forty different voltage settings, sweeping out the entire range of fission-fragment kinetic-energy-to-ionic-charge ratios.

In order to establish mass numbers the kinetic energy of the fragment must be known accurately. The energy of the fragment was measured in two ways – by transmission through the analyzer and by the surface-barrier detector. Any fragment subtended by the energy detector must have a kinetic energy E equal to kq, where q is the ionic charge of the fragment and k is the analyzer constant. The accuracy of the analyzer constant depended on the accuracy in constructing the radius of curvature, the electrode gap, the deflection angle, and in the alignment. The analyzer constant, of course, also depended on the high voltage supplied to the electrodes. The energy measured by the surface-barrier detector was determined by a mass dependent energy calibration scheme developed by Schmitt[18]). A calibration spectrum was obtained from the ^{252}Cf fission source in the detector chamber.

Kinetic-energy pulse-height spectra measured by the surface-barrier detector for three different voltage settings are shown in fig. 4. For the 71.070 kV setting, practically all the fragments belong to the light fission-fragment group; for the 46.487 kV setting, almost all the fragments belong to the heavy group. In both cases each peak of the energy spectrum corresponds to a unique charge state q whose kinetic energy is $kq(1\pm0.003$ fwhm) where k is the analyzer constant. For 55.239 kV appreciable amounts of both light and heavy fragments are present. Average pulse-height defects for the light and heavy fragments are such that each peak in the pulse-height spectrum corresponds to two kinetic energies, kq for the light group and $k(q+1)$ for the heavy group.

The pulse-height spectra were converted to kinetic energy spectra by using the Schmitt calibration procedure. Then, all events under an energy peak were assigned a discrete energy value kq. After establishing accurate energies for each event, masses were calculated from the time pulse height x_t and this energy. The following relationship was used:

$$m = ckq\,(fx_t+e)^2,$$

where c, f, and e are constants. The constant c incorporated the flight path squared and conversion constants. The constant f was determined approximately by time calibration. The constant e was based chiefly on the time delay cables and was approximated by measuring the length of cables. Once mass spectra were generated, more exact values of f and e were found by utilizing structure of the mass spectra.

For any given voltage setting events were sorted by energy. Mass distributions were generated for each of the energy peaks of the energy spectra. The mass distributions were then summed over all

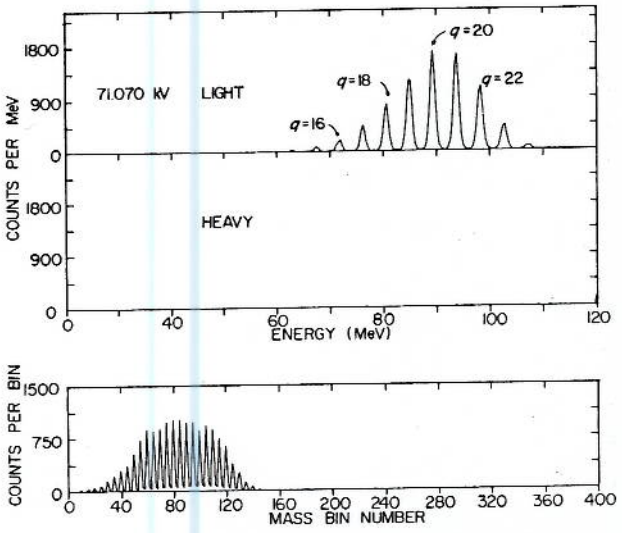

Fig. 5. Energy spectra for light and heavy fission fragments, and the mass distribution obtained for an analyzer high voltage setting of 71.070 kV.

energies to give a mass distribution for an electrostatic analyzer voltage setting. The number of counts under the peaks in the mass distributions were determined for all of the various cases.

3.2. Experimental results

The three figures which follow show experimental results for 3 of the 40 voltage settings used for the mass-yield measurement. The energy spectra for light and heavy fragments and the mass distribution obtained for an electrostatic analyzer high voltage of 71.070 kV is shown in fig. 5. This voltage setting selects only light fragments. The structure in the energy spectra is due to fragment

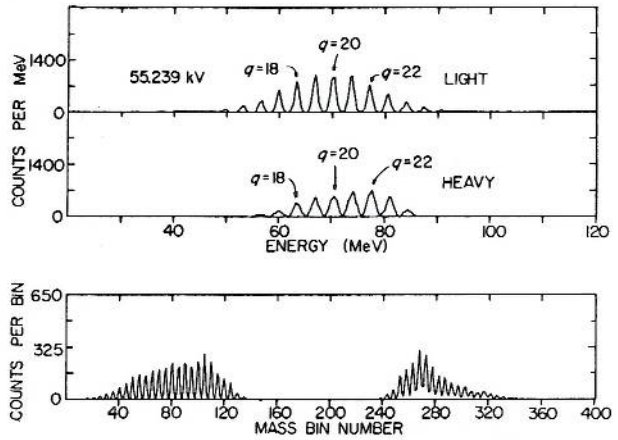

Fig. 6. Energy spectra for light and heavy fission fragments, and the mass distribution obtained for an analyzer high voltage setting of 55.239 keV.

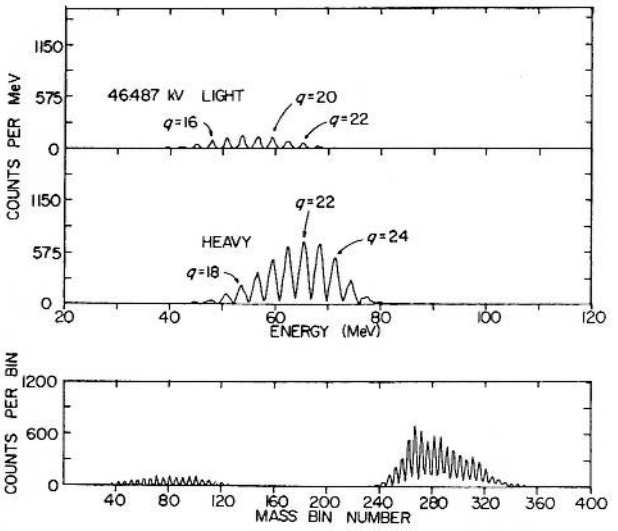

Fig. 7. Energy spectra for light and heavy fission fragments, and the mass distribution obtained for an analyzer high voltage setting of 46.487 kV.

charge states being integer. Each energy peak is associated with a different ionic charge but the ratio of energy to ionic charge is the same for all the energy peaks. Note that charge state separation is

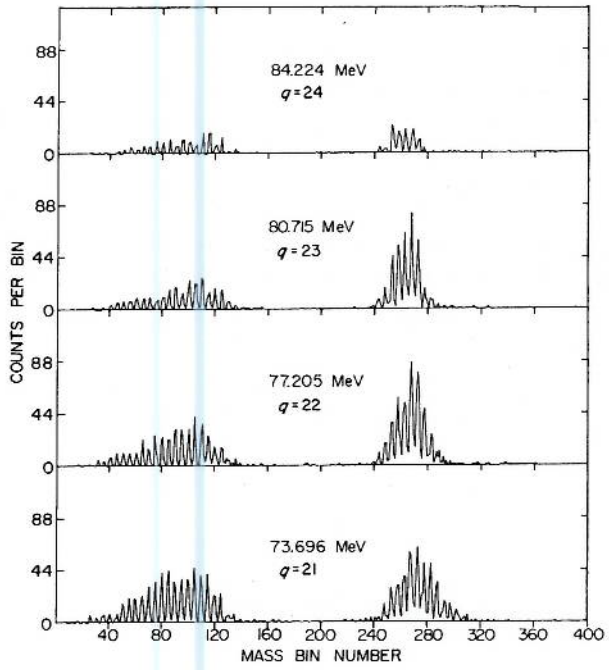

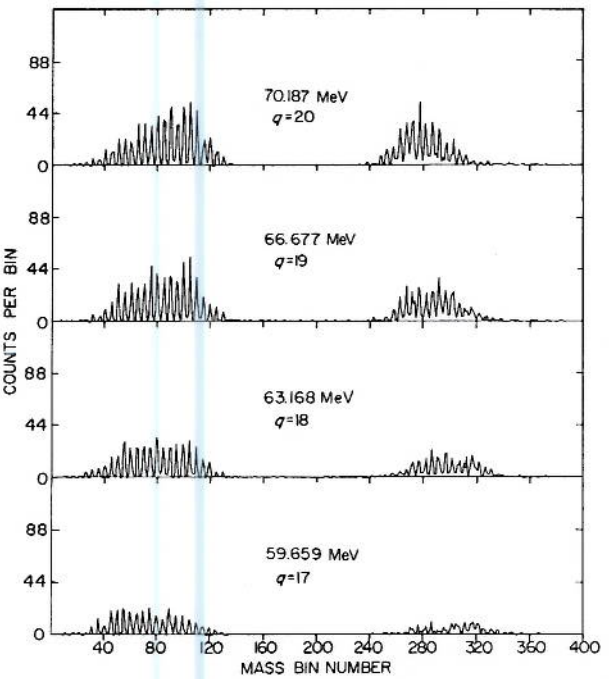

Fig. 8. Mass distributions obtained for events having a single energy for analyzer voltage of 55.239 kV. The energy given in each graph is determined from the electrostatic analyzer voltage setting.

better for the energy spectrum shown here than the pulse-height spectrum shown in fig. 4. This improvement is due to the use of the Schmitt calibration scheme. The structure in the mass distribution is due to individual masses and demonstrates a mass resolution of 0.5 amu or better. Fig. 6 shows energy spectra and the mass distribution obtained for an electrostatic analyzer high voltage of 55.239 kV, an intermediate setting. Fig.7 shows energy spectra and the mass distribution obtained for an electrostatic analyzer high voltage of 46.487 kV, a low setting which selects mostly heavy fragments.

Fig. 8 shows the mass distributions obtained for each of the principal energy peaks for the analyzer setting of 55.239 kV. The mass distribution shown in fig. 6 is the sum of all such mass distributions for the energy peaks shown in fig. 6. In order to obtain a complete description of the fission fragments measured by HIAWATHA, the sum of counts under each mass peak of all the mass distributions like the ones shown in fig. 8 was plotted as a function of the fragment energy and ionic charge – two-dimensional distributions for each mass. Two of the fifty distributions generated are shown in figs. 9 and 10. All of the distributions had the same general shape and exhibited some energy degradation due to the thick fission foil used.

In order to obtain mass yields in thermal fission of ^{235}U, the number of counts under each mass peak of the mass distributions generated for electrostatic analyzer high voltage settings (figs. 5–7) were plotted versus high voltage after adjustment for HIAWATHA transmission dependence on high voltage. Fig. 11b shows this normalized counting rate for several different masses while fig. 11a gives the observed counting rate at the surface-barrier detector due to all the fragment masses. The mass yields were obtained by integrating the area of a mass curve and taking the ratio of the area to the sum of the areas for all the masses of a group. The integration was performed by least squares fitting the data with a ninth order polynomial. For the light fission-fragment group the yields were calculated directly from the data as described above.

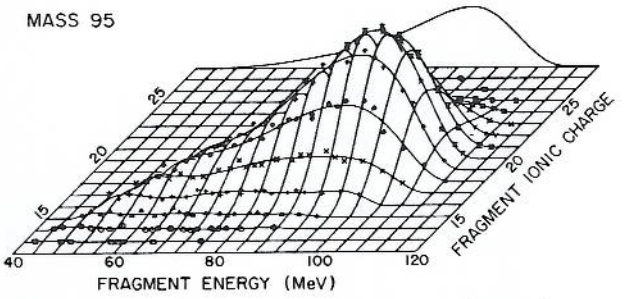

Fig. 9. Normalized counting rate for mass-95 fission fragment measured by HIAWATHA. The curve in the background is the kinetic energy distribution for mass 95, i.e., the sum (rescaled) of the kinetic energy distributions for each ionic charge state.

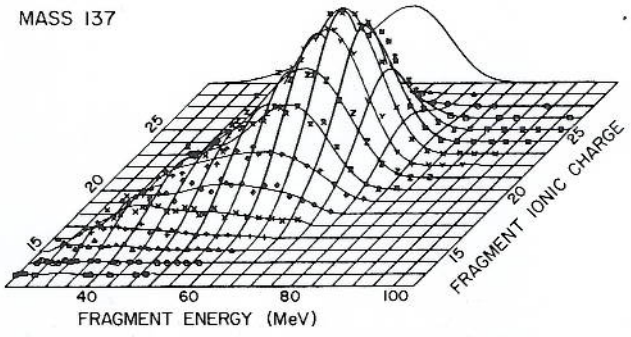

Fig. 10. Normalized counting rate for mass-137 fission fragment measured by HIAWATHA. The curve in the background is the kinetic energy distribution for mass 137, i.e., the sum (rescaled) of the kinetic energy distributions for each ionic

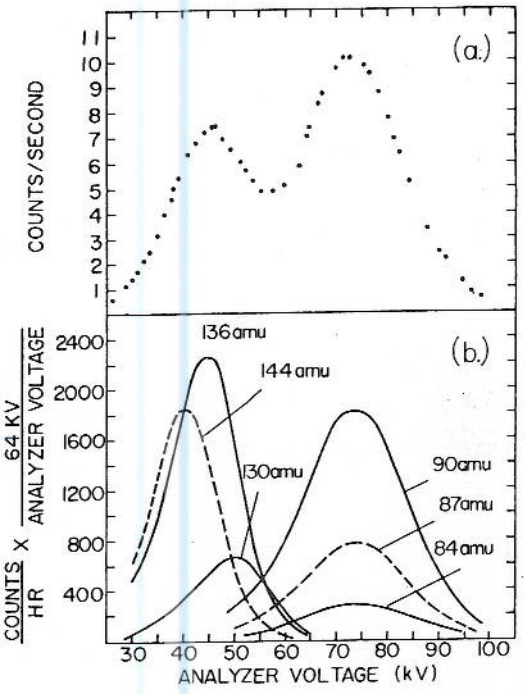

Fig. 11 (a) Fission fragment counting rate at the energy detector of HIAWATHA. (b) Normalized counts under selected

For the heavy fission-fragment group correction of the data was necessary. Because of incomplete energy separation for the heavy fragments, fig. 7, some charge states and hence mass numbers were misidentified. This effect was small and together with a background rate was corrected for. However, an apparent inefficiency of the system for the heavier, less energetic heavy fragments could not be compensated for directly. The heavy group was normalized against the evaluated yields of Meek and Rider[2]). By assuming the systematic errors in HIAWATHA are slowly varying in mass, a normalizing factor smoothly varying with mass was generated whose accuracy was established by the average of several evaluated yield values in a local mass range.

3.3. Mass yields in thermal fission of ^{235}U

The excellent mass resolution shown by the mass distributions obtained in the HIAWATHA measurements, $\sim\frac{1}{2}$ amu with complete separation for the light fragments and good separation of the heavy fragments, permitted the determination of mass yields in thermal-neutron fission of ^{235}U. The results are presented in fig. 12 as open points. The lines in this figure connect the evaluated chain yields of Meek and Rider[2]) for comparison. Our measurement is the first physical measurement of a fission mass distribution having good enough mass resolution to permit the accurate determination of mass yields.

Figs. 13 and 14 compare in detail the results of the HIAWATHA measurement with the Meek and Rider compilation. The points are the differences between the measured mass yields adjusted for delayed neutron emission and the chain yields of Meek and Rider. The error bars are the quadrature sum of the standard errors assigned to the HIAWATHA measured yields, the Meek and Rider evaluated yields, and delayed neutron yields. For the most part there is good agreement.

The errors assigned to the measured yields are based on counting statistics and were calculated as the square root of the total counts per mass. The error introduced by the polynomial least-squares fitting was investigated by using successively higher order polynomials and was shown to be insignificant. An additional error was introduced for the heavy fragments due to the normalization of the fragment yields. The error was estimated by computing the standard deviation of the data

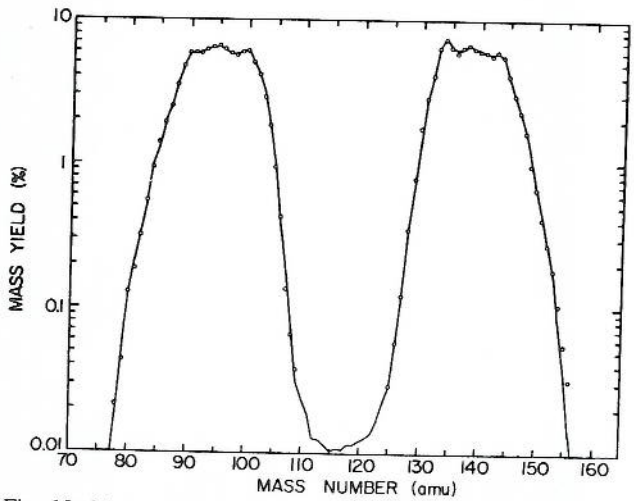

Fig. 12. Mass yields in thermal-neutron fission of ^{235}U. The circles are the results obtained using HIAWATHA and the lines connect the evaluated chain yields of Meek and Rider.

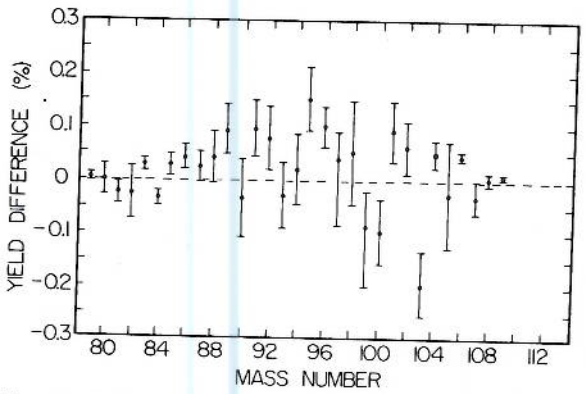

Fig. 13. Differences in mass yields–light fragments. The chain yields of Meek and Rider were subtracted from the measured yields which were adjusted for delayed neutron emission.

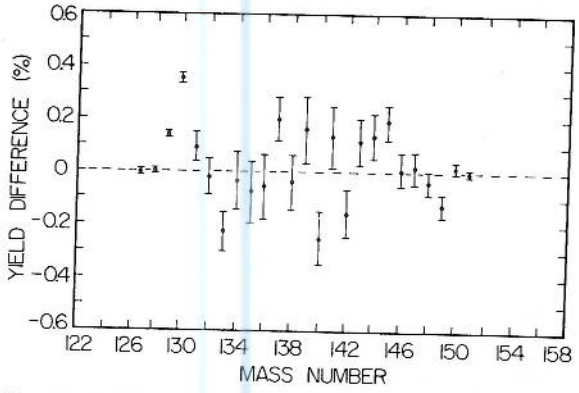

Fig. 14. Differences in mass yields – heavy fragments. The chain yields of Meek and Rider were subtracted from the measured yields which were adjusted for delayed neutron emission.

ts from the normalizing line for several data
ts near the mass of interest. Errors of about
per cent of the mass yields were found and
e added in quadrature to the errors determined
counting statistics.
he measured yields were adjusted for known
yed neutron emission because radiochemistry
mass spectrometry analyze fission products af-
delayed neutron emission, whereas HIAWA-
A, measures the fragments before delayed neu-
emission. The adjustment is not exact and
ably not complete. Currently, new neutron
ursors are being discovered and the accuracy
lelayed neutron yields, improved[19-21]).
he most pronounced disagreements between
asured and evaluated mass yields are for
ses 129 and 130, the differences being many
dard errors in value. No mass spectrometric
few radiochemical measurements have been
le for these two masses. It was concluded that
mass yields obtained by HIAWATHA for
s numbers 129 and 130 are significantly more
rate than those given by the Meek and Rider
pilation[2]).
he other discrepancies are small when com-
ed to the errors and may be due to systematic
rs associated with techniques of radiochemis-
and mass spectrometry, errors in data evalua-
, or errors in delayed neutron yields. Table 1
s measured mass yield results in disagreement
h Meek and Rider, and values from other com-
tions[1, 22-23]). It should be noted that the compi-
ons, using similar data bases, exhibit disagree-
nts among themselves. For masses 80 and 82
work is the first experimental determination of
se yields. Evaluated values for these yields
re based solely on interpolation of adjacent
lds.

. Neutron yield

The average number of neutrons emitted per fis-
n, $\bar{\nu}$, was derived from the fission-fragment
ss yield data[24]). The formula used is:

$$= A_0 - (\bar{A}_l + \bar{A}_h),$$

ere A_0 is the mass number of the compound
ile nucleus and $\bar{A}_l$ and $\bar{A}_h$ are the average mass
mbers for the light and heavy group respective-
The average mass values were calculated from
measured mass yields. The value for $\bar{\nu}$ was
termined for both pre-delayed neutron and post-
ayed neutron mass yields. The values obtained

Table 1

Mass yield results for those measured yields in disagreement with Meek and Rider.

Mass No.	Crouch[22])	Lammer & Eder[23])	Walker[1])	Meek & Rider[2])	Hiawatha[a])
95	6.45	6.54	6.50	6.46	6.61
103	3.03	2.95	3.12	3.14	2.94
129	1.0	0.64	0.65	0.66	0.80
130	2.0	2.00	1.7	1.46	1.81
133	6.72	6.73	6.75	6.77	6.56
140	6.32	6.37	6.36	6.32	6.07
145	3.87	3.91	3.93	3.94	4.13
149	1.01	1.05	1.07	1.09	0.97

[a] Adjusted for delayed neutron emission.

are: 2.46 ± 0.03 for pre-delayed neutron emission and 2.47 ± 0.03 for post-delayed neutron emission. The error assignment was based on the derivation of Zisin et al.[24]) and is dependent on the accuracy of the mass yield measurements. The post-delayed neutron value compares with the accepted value of 2.4220 ± 0.0066 recommended by Hanna et al.[25]).

3.5. Mass yields vs fragment energy

To test the feasibility of using HIAWATHA for studies of the dependence of fision yields on fis-

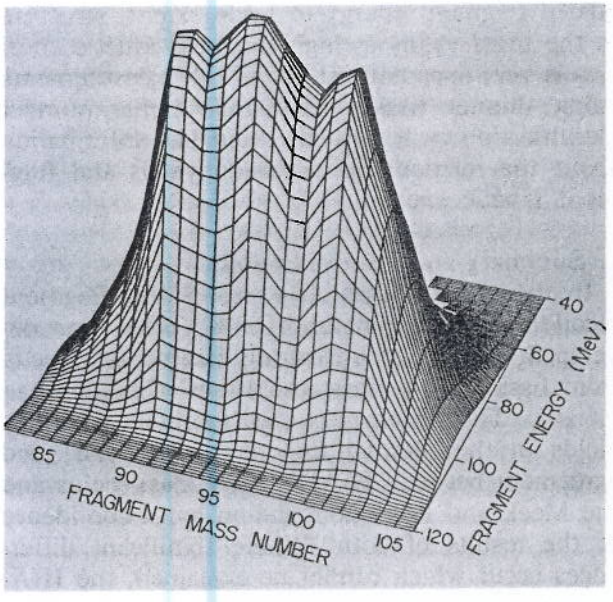

Fig. 15. Light fission-fragment mass yields in the thermal-neutron fission of ^{235}U. The energy axis gives the kinetic energy of the fragment after leaving the source foil.

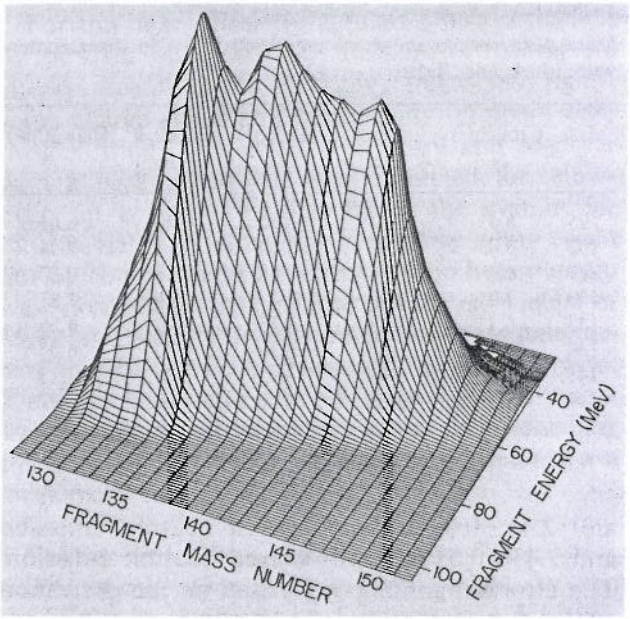

Fig. 16. Heavy fission-fragment mass yields in the thermal-neutron fission of ^{235}U. The energy axis gives the kinetic energy of the fragment after leaving the source foil.

sion energy, mass yields were determined as a function of fragment kinetic energy from the HIAWATHA data. The results are shown in figs. 15 and 16 for the light and heavy fission-fragment groups, respectively. Although the fission foil degraded fragment energy to some extent, structure in the mass yields at high fragment kinetic energies is very apparent. HIAWATHA measurements using thinner fission foils and atomic number identification will provide valuable information about the relationship of fission yields and fragment kinetic energy.

4. Summary and future research

In the present research a new fission-fragment recoil mass spectrometer, HIAWATHA, was developed capable of measuring fragments directly from fission with mass resolutions of better than 0.5 amu. The system was used to obtain the mass yields in the thermal fission of ^{235}U. The good agreement between HIAWATHA mass yields and the Meek and Rider compilation lends confidence to the results of both. Where significant differences occur which cannot be explained, the HIAWATHA yields are recommended.

HIAWATHA will be used to make absolute measurements of nuclide yields in fission. By incorporating an energy-loss detector near the surface-barrier detector, the atomic number of the fragment will be measured simultaneously with the mass number of the fragment. Experimental data measured by us[26]) and experiments conducted at the Lohengrin facility[11]) indicate that approximately one-Z atomic number resolution is possible by use of the energy-loss technique. The energy-loss chamber, to be used with HIAWATHA, is a thin windowed gas ionization chamber. The experiment will be conducted in a similar manner to the mass-yield measurement except for the additional parameter of energy loss.

In principle, fission yield measurements could be performed on any fissile material for any neutron energy distribution, but, in practice, are limited by the available fission rate at the source. Practical measurements that can be performed at the Illinois Advanced TRIGA facility are the thermal-neutron fission yields of ^{235}U, ^{239}Pu and ^{233}U. Fast fission measurements would require fast neutron fluxes of about 10^{14} n/cm^2·s and could only be performed at a suitable facility.

Information other than fission-yield data can be determined from HIAWATHA experiments. Ionic charge state distributions of fission fragments after passage through absorbers can be found as a function of atomic number, mass, and energy. An improved surface-barrier detector energy calibration will be investigated. Studies of heavy-ion channeling in crystals can be performed over the fragment mass and energy range. Fission-fragment energy loss and straggling as a function of atomic number and velocity are being investigated.

Appreciation is expressed to G. Beck, P. Hesselmann, C. Pohlod, D. Sigler, and R. Coon for their help in reactor operations; to L. Stalker and C. Luesse for their care in constructing the experimental equipment; to R. Bucher for his aid in constructing a reliable four-parameter analyzer; to D. Ingersoll, N. Hertel, and R. Lipinski for their assistance and helpful discussions; and to R. Strittmatter for his aid and for continuing the work with HIAWATHA. The authors are also indebted to S. Bashkin for supplying the carbon foils; to C. Crouch of Harwell, O.J. Eder of the Institut für Physik, Vienna, W.J. Maeck of Allied Chemical, Idaho, and B.F. Rider of General Electric for their helpful comments on the mass-yield results.

References

1) W. H. Walker, Chalk River Nuclear Laboratories, Chalk River, Ontario, AECL-3037 (1973).
2) M. E. Meek and B. F. Rider, Vallecitos Nuclear Center, NEDO-12154-1 (1974).
3) G. DiIorio and B. W. Wehring, Trans. Am. Nucl. Soc. **23** (1976) 523.
4) H. W. Schmitt, W. E. Kiker and C. W. Williams, Phys. Rev. **137** (1965) B837.
5) F. Shiraishi and M. Hosoe, Nucl. Instr. and Meth. **66** (1968) 130.
6) M. Derengowski and E. Melconian, Phys. Rev. C **2** (1970) 1554.
7) G. DiIorio and B. W. Wehring, Trans. Am. Nucl. Soc. **24** (1976) 459.
8) S. Borg and I. Bergstrom, Nucl. Instr. and Meth. **91** (1971) 109.
9) U. A. Arifov, A. D. Belyaev, V. I. Kogan, V. P. Pikul and A. M. Usmandiyarov, Sov. Phys. **17**, no. 5 (1972) 485.
10) E. Moll, H. Schrader, G. Siegert, M. Asghar, J. P. Bocquet, G. Bailleul, J. P. Gautheron, J. Greif, G. I. Crawford, and C. Chauvin; E. Ewald and H. Wollnik; P. Armbruster, G. Fiebig, H. Lawin and K. Sistemich, Nucl. Instr. and Meth. **123** (1975) 615.
11) H. G. Clerc, K. H. Schmidt, H. Wohlfarth, W. Lang, H. Schrader, K. E. Pferdekämper, R. Jungmann, M. Asghar, J. P. Bocquet and G. Siegert, Nucl. Phys. **A247** (1975) 74.
12) C. W. Williams and J. A. Biggerstaff, Nucl. Instr. and Meth. **25** (1964) 370.
13) W. F. W. Schneider, B. Kohlmeyer and R. Bock, Nucl. Instr. and Meth. **87** (1970) 253.
14) E. Dietz, J. Czarnecki, W. Patscher, W. Schafer, and R. Bass, Nucl. Instr. and Meth. **108** (1973) 607.
15) C. D. Moak, H. O. Lutz, L. B. Bridwell, L. C. Northcliffe and S. Datz, Phys. Rev. Lett. **18** (1967) 41.
16) H. Wollnick, *Focusing of charged particles* (ed. A. Septier; Academic Press, New York, 1967) vol. 2, p. 163.
17) C. W. Williams, W. E. Kiker and H. W. Schmitt, Rev. Sci. Instr. **35** (1964) 1116.
18) H. W. Schmitt, W. M. Gibson, J. H. Neiler, F. J. Walter and T. D. Thomas, Proc. IAEA Conf. on *The physics and chemistry of fission* (1965) paper SM-60/40, vol. 1, p. 531.
19) T. Izak-Biran and S. Amiel, Nucl. Sci. Eng. **57** (1975) 117.
20) M. Asghar, J. P. Gautheron, G. Bailleul, J. P. Bocquet, J. Greif, H. Schrader and G. Siegert, Nucl. Phys. **A247** (1975) 359.
21) G. Rudstam and E. Lund, Phys. Rev. **C13** (1976) 321.
22) E. A. C. Crouch, IAEM/SM-170/94, Symp. on *Applications of nuclear data in science and technology,* Paris 1973.
23) M. Lammer and O. J. Eder, IAEA/SM-170/13, Symp. on *Applications of nuclear data in science and technology,* Paris (1973).
24) Yu. A. Zisin, A. A. Lbov and L. I. Sel'Chenkov, J. Nucl. Energy Parts A/B **17** (1963) 41.
25) G. C. Hanna, C. H. Westcott, H. D. Lemmel, B. R. Leonard, Jr., J. S. Story and P. M. Atree, At. Energy Rev. **7** (1969) 4.
26) B. W. Wehring and R. G. Bucher, Proc. 4th Int. Conf. on *Beam-foil spectroscopy and heavy-ion atomic physics,* Gatlinburg, Tenn. (1975) (Plenum, New York, 1976) pp. 679-686.